



HAL
open science

Steroid/mucokinetic hybrid nanoporous microparticles for pulmonary drug delivery

Frederic Tewes, Krzysztof J. Paluch, Lidia Tajber, Karan Gulati, Devesh Kalantri, Carsten Ehrhardt, Anne Marie Healy

► **To cite this version:**

Frederic Tewes, Krzysztof J. Paluch, Lidia Tajber, Karan Gulati, Devesh Kalantri, et al.. Steroid/mucokinetic hybrid nanoporous microparticles for pulmonary drug delivery. *European Journal of Pharmaceutics and Biopharmaceutics*, 2013, 85 (3), pp.604-613. 10.1016/j.ejpb.2013.03.020 . inserm-01102852

HAL Id: inserm-01102852

<https://inserm.hal.science/inserm-01102852>

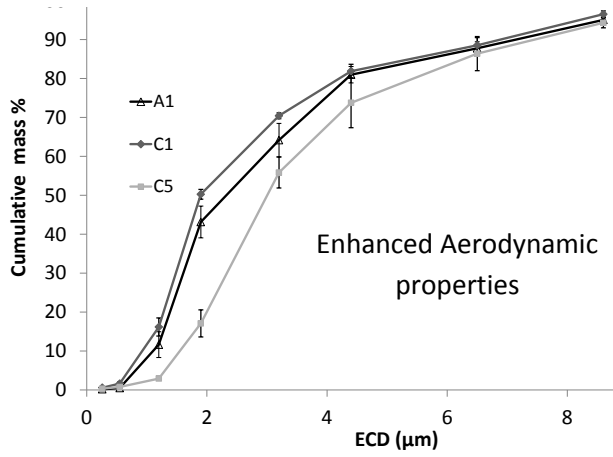
Submitted on 13 Jan 2015

HAL is a multi-disciplinary open access archive for the deposit and dissemination of scientific research documents, whether they are published or not. The documents may come from teaching and research institutions in France or abroad, or from public or private research centers.

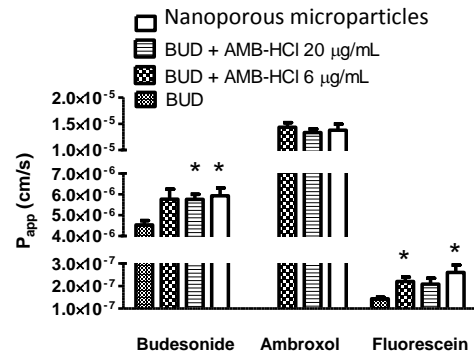
L'archive ouverte pluridisciplinaire **HAL**, est destinée au dépôt et à la diffusion de documents scientifiques de niveau recherche, publiés ou non, émanant des établissements d'enseignement et de recherche français ou étrangers, des laboratoires publics ou privés.



Budesonide-Ambroxol composite
Nanoporous microparticles
for DPI



Enhanced budesonide diffusion within mucous



Steroid/mucokinetic Hybrid Nanoporous Microparticles for Pulmonary Drug Delivery

Frederic Tewes^{1,2}, Krzysztof J. Paluch¹, Lidia Tajber¹, Karan Gulati¹, Devesh Kalantri¹, Carsten Ehrhardt¹ and Anne Marie Healy^{1,*}

1. School of Pharmacy and Pharmaceutical Sciences, Trinity College Dublin, Panoz Institute, Dublin 2, Ireland.
2. INSERM U 1070, Pôle Biologie-Santé, Faculté de Médecine & Pharmacie, Université de Poitiers, 1 rue Georges Bonnet, 86000 Poitiers, France.

* To whom correspondence should be sent. Ph.: +353 1 896 1444, e-mail: healyam@tcd.ie

Abstract

In a number of pulmonary diseases, patients may develop abnormally viscous mucus reducing drug efficacy. To increase budesonide diffusion within lung fluid, we developed nanoporous microparticles (NPMPs) composed of budesonide and a mucokinetic, ambroxol hydrochloride, to be inhaled as a dry powder. Budesonide:Ambroxol-HCl particles were formulated by spray drying and characterised by various physicochemicals methods. Aerodynamic properties were evaluated using a cascade impactor. Drugs apparent permeability coefficients were calculated across mucus producing Calu-3 cell monolayers cultivated at an air-liquid interface. Microparticles made only from budesonide and ambroxol-HCl had smooth surfaces. In the presence of ammonium carbonate ((NH₄)₂CO₃), NPMPs were formulated, with significantly ($P<0.05$) superior aerodynamic properties (MMAD=1.87±0.22 µm and FPF=84.0±2.6%). The formation of nanopores and the increase in the specific surface area in the presence of (NH₄)₂CO₃ was mainly attributed to the neutralisation of Ambroxol-HCl to form ambroxol base. Thus, ambroxol base could behave in the same manner as budesonide and prompt nanoprecipitation when spray dried from an ethanol/water mix occurs. All formulations were amorphous, which should enhance dissolution rate and diffusion through lung fluid. These NPMPs were able to improve budesonide permeability across mucus producing Calu-3 cell monolayers ($P<0.05$) suggesting that they should be able to enhance budesonide diffusion in the lungs through viscous mucus.

Keywords: Budesonide; Ambroxol; Nanoporous microparticles; Calu-3 cells; Andersen cascade impactor; Dry powder inhaler.

1. Introduction

Pharmacotherapy of lung diseases often involves treatment with more than one group of therapeutic agents (e.g., bronchodilators, corticosteroids, cromoglycate, and antibiotics). In addition to the oral route, these agents are often delivered by pulmonary inhalation, in order to directly target the lung and increase the therapeutic/systemic side effect index.

The local delivery of drugs to the lung can be obtained by using dry powder inhalers (DPIs), metered dose inhalers (MDIs) or nebulisers. Whenever it is possible, the use of DPIs or MDIs is preferred by patients due to the convenience of use [1, 2]. The simplest formulation and least problematic, from the point of view of stability, appears to be dry powders due to the presence of the active pharmaceutical ingredient (API) as solid particles and the lack of propellant, in contrast to pressurised MDIs, where the API is dissolved or suspended in the liquefied vehicle [3]. Also, in order to improve the results of pharmacotherapy, increase patient compliance and reduce the time of administration of several APIs, co-formulation of drugs into one product [4-7] or co-administration of drugs as a mix of solutions for nebulisation is popular. However, the latter can bring the risk of physicochemical instability of components when mixed extemporaneously [8].

To optimise the efficacy of DPIs, conventional micronised API carrier-based formulations may be substituted by an optimised API powder having specific particle morphology and designed to provide advantageous flow and aerodynamic properties. For example, tobramycin powder was produced using emulsion-based PulmoSphere technology, producing highly dispersible porous particles [9]. Excipient-free nanoporous microparticles (NPMPs) [10] of budesonide (BUD) [11] and sodium cromoglycate [12] prepared by a novel spray drying process had improved *in vitro* deposition properties compared to non-porous particles, though it remained unknown, if it is possible to produce NPMPs composed of two APIs and still be able to maintain

the superior aerodynamic properties.

BUD was previously reported to form NPMPs when processed by spray drying [11]. BUD is a glucocorticosteroid which, when inhaled, has a dose-dependent anti-inflammatory action in the lung [13]. It acts by binding to glucocorticoid receptors in lung cell cytoplasm [14]. Budesonide has been shown to be very effective against the characteristic inflammation of asthma [15]. It is reported to reduce the risk of Chronic Obstructive Pulmonary Disease (COPD) exacerbations in symptomatic COPD patients [16]. Budesonide also resulted in an improvement in bronchial hyper-responsiveness and a decrease in cough in cystic fibrosis patient [17]. However, in these two last diseases, efficacy of inhaled corticosteroids can be strongly reduced because of the low diffusion through the viscous surface secretions of the lung [18]. In fact, in a number of pulmonary diseases, patients may develop abnormally high viscous thick mucus which is responsible for low diffusion of drugs in the lungs [5, 19, 20].

To reduce the viscosity of the lung fluid, mucokinetics such as ambroxol hydrochloride (AMB-HCl) are used [21]. Ambroxol may provide suitable rheological properties of the airway secretion by acting directly on ciliated epithelial cells [22]. Ren *et al.*, [23] showed that the rat lung epithelial lining fluid (ELF)/plasma AUC_{0-10h} ratios obtained for ambroxol hydrochloride (AMB-HCl) after dry powder pulmonary administration were 33 to 56 times higher compared to those achieved by intravenous administration. Thus, the co-administration of BUD together with AMB-HCl could possibly improve the diffusion of BUD in the lining fluid of the lung and enhance its bioavailability. For that reason, we developed a combined BUD AMB-HCl formulation as excipient-free NPMPs to be used in DPIs.

2. Materials and methods.

2.1. Materials

Budesonide (BUD) was purchased from Tianjin Tian Mao Technology Development Corp. Ltd., China. Acetonitrile (HPLC grade), ambroxol hydrochloride (AMB-HCl) and ammonium carbonate $(\text{NH}_4)_2\text{CO}_3$ (analytical grade) were purchased from Sigma-Aldrich (Dublin, Ireland). Ultrapure water was produced by a Synergy Ultrapure Water System linked to an Elix Advantage system (Millipore, Carrigtwohill, Ireland). Sodium pyruvate, foetal calf serum (FCS), non-essential amino acids solution (NEAA), minimum essential medium (MEM), glucose, penicillin/streptomycin solution, NaCl, KCl, CaCl_2 , $\text{MgCl}_2 \cdot 6 \text{H}_2\text{O}$, NaHCO_3 and HEPES were cell culture grade and purchased from Sigma-Aldrich.

2.2. Methods

2.2.1. Spray drying

Spray drying experiments were performed based on methods described by Nolan *et al.* [11]. Briefly, 1% (w/w) solutions of different BUD:AMB-HCl ratios, with and without $(\text{NH}_4)_2\text{CO}_3$ (Table 1), were spray dried using a Büchi B-290 Mini spray dryer (Flawil, Switzerland) from a solvent made of 80% (v/v) ethanol and 20% (v/v) water. The spray dryer was set in an open suction mode using a standard two-fluid nozzle. In all cases the inlet temperature was 78°C; feeding pump was set at 30% (8 mL/min); spraying nitrogen nozzle flow rate was 15 L/min; and nitrogen flowing at 630 L/min was used as the drying gas (aspirator rate 100%). These conditions resulted in outlet temperatures ranging from 42 to 52°C.

Table 1: Total content of solids materials (% w/w) used to prepare the feed solutions (1 % w/v).

Compounds	Solid content % (w/w)										
	With (NH ₄) ₂ CO ₃								Without (NH ₄) ₂ CO ₃		
	C1	C2	C3	C4	C5	C6	C7	C8	A1	A2	A3
BUD	80	75	70	65	65	55	45	33	95	90	80
AMB-HCl	5	10	15	20	10	10	20	33	5	10	20
(NH₄)₂CO₃	15	15	15	15	25	35	35	33	0	0	0

2.2.2. Scanning electron microscopy (SEM)

Scanning electron micrographs of powder samples were taken using a Tescan Mira XMU (Brno, Czech Republic) SEM. The dry powder samples were fixed on aluminium stubs with double-sided adhesive tape and a 10 nm-thick gold film was sputter coated on the samples, before visualisation. Primary electrons were accelerated under a voltage of 5 kV. Images were formed from the collection of secondary electrons.

2.2.3. Specific surface area

The specific surface area of the samples was determined by the N₂ adsorption B.E.T. multipoint method, with 6 points in the relative pressure range of 0.1–0.3, using a Micromeritics Gemini 2835c (SMS Ltd., London, UK) as previously described [11]. Samples were prepared by purging under N₂ overnight at 40 °C.

2.2.4. Particle size distribution analysis

The geometric particle size distributions (PSD) were determined by laser diffraction using a Malvern Mastersizer 2000 (Malvern Instruments Ltd. Worcestershire, UK) with the Scirocco 2000 dry powder feeder to disperse the particles. The dispersive air pressure used was 3 bar and vibration feed rate was set to 50%. The PSD of each sample was determined in triplicate.

2.2.5. Differential scanning calorimetry (DSC)

DSC was performed using closed 40 μL -aluminium pans with three vent holes on samples (4 – 8 mg) weighed with a MT5 balance (Mettler Toledo, Zürich, Switzerland) [24]. Samples were run at a heating rate of $10^\circ\text{C}/\text{min}$ under nitrogen purge from 40°C to 270°C using a Mettler Toledo DSC 821^e (Switzerland). Mettler Toledo STAR^e software was used for analysis of thermal events.

2.2.6. Powder X-Ray Diffraction (XRD)

X-ray powder diffraction measurements were conducted on samples placed in a low background silicon holder, using a Miniflex II desktop X-ray diffractometer (Rigaku, Tokyo, Japan) with a Bragg-Brentano geometry [24, 25]. The samples were scanned over a range of $5 - 40^\circ 2\theta$ at a step size of 0.05° per second. The X-ray tube composed of copper anode was operated under a voltage of 30 kV and a current of 15 mA, which, after crossing a monochromator, produced copper $K\alpha$ radiation ($\lambda = 1.542 \text{ \AA}$). A scintillation counter detected the X-rays.

2.2.7. Drug quantification

A HPLC method, based on the method described by Nolan *et al.* [11] was set up to assay both BUD and AMB-HCl simultaneously. The assay was performed using a LC module I plus (Waters, UK) chromatographic system equipped with a C18, 15-20 μm , 3.9 x 300 mm apolar column ($\mu\text{Bondapak}^{\text{TM}}$, Waters, Ireland). Drug elution was detected by measuring the absorbance at 242 nm. Measurements were conducted at room temperature by injecting 50 μL of samples, standards or controls in the mobile phase running at 1.5 mL/min and composed of 55% by volume of 0.05 M $\text{CH}_3\text{COOH}/\text{Na}$ buffer (pH 4) and 45% of acetonitrile. The running time of the assay was 7 min. A calibration curve for each drug was constructed, allowing the drug concentrations in samples to be calculated. The concentration of the standard solutions of each drug used to construct the calibration curves were in the range 6 $\mu\text{g}/\text{mL}$ to 100 $\mu\text{g}/\text{mL}$.

2.2.8. In Vitro Deposition Studies Using the Andersen Cascade Impactor (ACI)

A dry powder inhaler (Cyclohaler[®], N.V. Medicopharma, Zaandam, Netherlands) was filled with a size 3 hard gelatin capsule loaded with 20±2 mg of powder for each test. After inhaler actuation, particle deposition in the device, the induction port, all the stages and the filter was determined by the HPLC assay described above (n=3). The flow rate (60 L/min) used in the ACI. The time of aspiration was adjusted to obtain 4 L. The total amount of particles with aerodynamic diameters smaller than 5.0 µm was calculated by interpolation from the inverse of the standard normal cumulative mass (mg) distribution less than stated size cut-off against the natural logarithm of the effective cut-off diameter (ECD) of the respective stages. This amount was considered as the fine particle fraction (FPF). The mass median aerodynamic diameter (MMAD) of the particles was defined from a similar plot, but using the cumulative mass fraction (%) against the ECD of the respective stage, as the particle size at which the line crosses the 50% mark.

2.2.9. BUD and AMB transport across Calu-3 cell monolayers

Calu-3 human bronchial epithelial cells were cultured in Eagle's minimum essential medium supplemented with 1 mM of sodium pyruvate, 10% (v/v) foetal calf serum, 1% (v/v) non-essential amino acids, 2.25 g/L glucose and 1% (v/v) penicillin/streptomycin, and were used between passages 38 and 55. Cells were cultured in 75 cm² flasks and maintained in a humidified atmosphere of 5% CO₂ and 37 °C. Cell monolayers were obtained by seeding Calu-3 cells (5 × 10⁵ cells/cm²) onto polyester Transwell Clear inserts, with 0.4 µm pore diameter and 1.12 cm² of surface area (Corning, Netherlands). Growth medium, 1.5 mL on the basal side compartment and 0.5 mL on the apical side, was replaced with fresh medium every other day.

A) A first set of experiments was conducted as follows: After 10 days in culture, the culture medium on the apical side was removed and cells were grown under air-interfaced culture (AIC) conditions for another 10 days. These culture conditions have previously shown to induce

the production of mucus by Calu-3 cells [26, 27]. Transport experiments were carried out in a HEPES-buffered Krebs-Ringer solution (KRB; 150 mM NaCl, 5.2 mM KCl, 2.2 mM CaCl₂, 0.2 mM MgCl₂ 6•H₂O, 6 mM NaHCO₃, 5 mM HEPES, 2.8 mM glucose; pH = 7.4). The basal side of the Calu-3 monolayers was equilibrated with KRB for 1 h prior to the transport study. Transport studies were initiated by adding to the apical side 0.8 mL of the test solutions containing fluorescein (10 µg/mL) and BUD (20 µg/mL) with or without AMB-HCl. A sample of this solution (0.3 mL) was then immediately removed for determination of the initial concentration. After 3 h at 37°C, samples were collected from the acceptor and donor compartments and assayed for BUD, AMB-HCl and fluorescein content.

B) A second set of experiments was performed as follows: 6 Transwell Clear filters were cultured under liquid-covered culture (LCC) conditions for 15 days. Six additional filter inserts were cultured in AIC conditions for 12 days after 3 days in LCC conditions. Transport experiments were carried out in Hank's balanced salt solution (HBSS) supplemented with 5 mM HEPES. For LCC conditions, basal and apical sides of the Calu-3 monolayers were equilibrated with HBSS for 1 h prior to the transport study. For AIC conditions, the basal side of the Calu-3 monolayers were equilibrated with HBSS for 1 h prior to the transport study. For both AIC and LCC conditions, transport studies were initiated by adding to the apical side 0.5 mL of the test solutions containing BUD (20 µg/mL) with or without AMB-HCl (20 µg/mL). After 3 h at 37°C, samples were collected from the acceptor and donor compartments and assayed for BUD and AMB-HCl.

BUD and AMB-HCl were assayed using the chromatographic method described above. Fluorescein was assayed using a 96-well plate reader (FLUOstar OPTIMA, BMG Labtech, Aylesbury, UK) by measuring the fluorescence intensity at 520 nm after excitation at 492 nm.

Standard solutions of fluorescein were made in KRB with concentration ranging from 0.015 $\mu\text{g/mL}$ to 1 $\mu\text{g/mL}$. Correlation coefficient of the calibration curves were higher than 0.99.

The apparent permeability (P_{app}) values in the apical-to-basal direction were calculated using the following equation:

$$P_{app} = \frac{C_b \cdot V_b}{A \cdot t \cdot C_a} \quad (1)$$

where C_b was the solutes concentration and V_b the volume (1.5 mL) of buffer in the basal side, t the incubation time (180 min) and A the insert surface area (1.12 cm^2). C_a was the initial concentration in the apical side.

2.2.10. Statistical data analysis

Data were statistically evaluated by a two-tailed unpaired Student t -test. Significance level was $\alpha < 0.05$.

3. Results

Spray drying of formulations A1-A3 resulted in the production of discrete and non-porous microparticles, having smooth surfaces (Fig. 1). Microparticle morphology depended on the BUD:AMB-HCl ratio. At low AMB-HCl concentrations (A1-A2) the particles were crumpled. An increase in AMB-HCl concentration (A3) led to particles with more spherical morphology.

Figure 1: SEM of particles made of BUD and AMB-HCl as described in Table 1.

The addition of 15% (w/w) of $(\text{NH}_4)_2\text{CO}_3$ altered the morphology of microparticles (Fig. 2). Most particles appeared to be porous with rough surfaces. At a constant $(\text{NH}_4)_2\text{CO}_3$ concentration of 15% (w/w) (C1 to C4) an increase in AMB-HCl concentration reduced the number of porous microparticles visible on SEM micrographs. Similarly, the specific surface area measured by N_2 adsorption decreased from $6.50 \pm 0.14 \text{ m}^2/\text{g}$ for C1 to $2.53 \pm 0.05 \text{ m}^2/\text{g}$ for C4, respectively. When the content of AMB-HCl was held constant (C2, C5, C6 and C4, C7), a small increase in $(\text{NH}_4)_2\text{CO}_3$ concentration (from 15% to 25% (w/w)), increased the number of pores visible by particles (Fig. 2: C2, C5) and increased the specific surface area from $5.67 \pm 0.08 \text{ m}^2/\text{g}$ for C2 to $7.14 \pm 0.17 \text{ m}^2/\text{g}$ for C5, respectively. However, a larger increase in $(\text{NH}_4)_2\text{CO}_3$ concentration (i.e., 35% w/w) produced hollow particles (Fig. 2: C6 and C7) and reduced the specific surface area to $3.91 \pm 0.06 \text{ m}^2/\text{g}$ for C6.

Figure 2: SEM and specific surface area values of the particles formulated in presence of $(\text{NH}_4)_2\text{CO}_3$ as described in Table 1. Error bars in the histogram correspond to the standard deviation of the specific surface area values calculated from 3 measurements.

Selected data of the geometric volume-weighted particles size analysis of the powders formulated using $(\text{NH}_4)_2\text{CO}_3$ are displayed in Table 2. The different formulations had similar particle size distributions. However, an increase in AMB-HCl or in $(\text{NH}_4)_2\text{CO}_3$ increased the median value of

the particle diameter (D_{50}) and widened the range of the particle size distribution, as shown by an increase in the span value. The specific surface area of the powder of formulation C4, calculated from the particle size distribution, considering the particles to be non-porous, was similar to the one calculated from the N_2 adsorption isotherm using the B.E.T. equation. However, B.E.T analysis for C5 gave a specific surface area value which was 2.3 times higher than that calculated from the particle size distribution. This difference can be attributed to the presence of pores in C5 and not in C4.

Table 2: Geometric volume-weighted particle size analysis

	D_{50} (μm)	SPAN	Specific Surface Area of particles calculated as smooth spheres (m^2/g)
C1	2.4 \pm 0.3	1.75 \pm 0.05	3.19 \pm 0.31
C2	2.6 \pm 0.2	1.70 \pm 0.1	2.94 \pm 0.28
C4	3.0 \pm 0.3	2.20 \pm 0.15	2.52 \pm 0.34
C5	2.6 \pm 0.3	1.67 \pm 0.09	3.07 \pm 0.30
C6	2.8 \pm 0.4	1.70 \pm 0.15	3.06 \pm 0.35
C7	4.6 \pm 1.1	2.90 \pm 0.62	1.98 \pm 0.46

Unprocessed materials, i.e., AMB-HCl, $(\text{NH}_4)_2\text{CO}_3$ and BUD presented sharp XRD Bragg peaks characteristic of crystalline compounds (Fig. 3). After spray drying, PXRD patterns of pure BUD and AMB-HCl presented a diffuse halo, characteristic of XRD amorphous materials, centred at 15 and 22.5° (2θ), respectively. In the presence of $(\text{NH}_4)_2\text{CO}_3$, one diffraction peak at $2\theta = 32.65^\circ$ appeared in the PXRD pattern of the AMB-HCl/ $(\text{NH}_4)_2\text{CO}_3$ 3/7 (w/w) spray dried system in addition to the diffuse halo (Fig. 3).

Figure 3: PXRD patterns of the raw and spray dried materials.

DSC analysis of unprocessed BUD and AMB-HCl confirmed powders to be crystalline with melting endotherm point onsets at 247°C and 242°C, respectively (Fig. 4). Spray dried BUD and AMB-HCl DSC scans displayed a relaxation endotherm of a glass transition (T_g) with onsets of

approximately 86-88°C, characteristic of amorphous materials. These powders were thermally unstable and crystallised upon heating, showing an exotherm with an onset at 124°C and 149°C for BUD and AMB-HCl, respectively (Fig. 4).

Figure 4: DSC thermograms of the unprocessed and spray dried materials. Insert in the figure is a magnified view of the spray dried AMB-HCl thermogram in the region of the T_g. The melting endotherm observed for DSC crystallised BUD shifted to an onset of 260°C. Unprocessed and spray dried AMB-HCl presented similar melting endotherms. DSC scans of AMB-HCl/(NH₄)₂CO₃ 3/7 (w/w) spray dried system presented four endotherms having the following temperature onsets: 60, 90, 98 and 229°C (Fig. 4).

Figure 5: PXRD patterns of the formulations as described in Table 1.

Formulations made of various BUD:AMB-HCl ratios (A1-A3) presented only a diffuse halo on their PXRD patterns (Fig. 5). The centre of the diffuse halo shifted from 15° (2θ) to higher values as the BUD:AMB-HCl ratio decreased. PXRD patterns of BUD:AMB-HCl formulations spray dried in the presence of (NH₄)₂CO₃ (C1-C8) displayed a diffuse halo that became broader as the BUD:AMB-HCl ratio decreased. Furthermore, a diffraction peak with increasing intensity as the AMB-HCl concentration increased appeared at 2θ = 32.6°. The intensity of this diffraction peak was independent of the (NH₄)₂CO₃ concentration.

Figure 6: Thermograms of the powders formulated without (A) and with (B) (NH₄)₂CO₃.

The thermograms recorded for the formulations A1 to A3 (Fig. 6A) displayed an onset of T_g at around 90°C, followed by one exotherm of crystallisation and two endotherms of melting. The temperature onsets and ΔH of these thermal events changed with the BUD:AMB-HCl ratio as shown in Supplementary data 1.

Supplementary data 1: Thermal event values for the BUD/AMB-HCl systems obtained by DSC.

Sample	Tg onset	Exotherm		Endotherm 1		Endotherm 2	
	[°C]	[°C]	[J/g]	[°C]	[J/g]	[°C]	[J/g]
A1	90	126	35	197	-9	239	-40
A2	90	130	33	193	-18	230	-18
A3	90	135	29	198	-2	205	-66
C1	NA	122	29	245	-72	NA	
C2	NA	129	35	226	-83	NA	
C3	NA	117	26	206	-2	228	-71
C4	NA	116	23	206	-7	226	-50
C5	NA	128	32	226	-68	NA	
C6	NA	122	29	226	-54	NA	
C7	NA	115	22	200	-11	223	-71
C8	NA	115	13	197	-50	NA	
BUD	NA	N/A	N/A	247	-67	NA	
AMB-HCl	NA	N/A	N/A	242	-92	NA	
Spray dried BUD	88	124	43.55	260	-87	NA	
Spray dried AMB-HCl	88	149	41.7	242	-92	NA	

At low AMB-HCl concentrations (formulation A1 and A2), two distinguishable endotherms (i.e., individual peaks) were observed. As the AMB-HCl concentration increased, the endotherms became closer and were followed by a noisy baseline, which could be attributed to product degradation. Also, DSC analysis of physical mixes of BUD:AMB-HCl in the range of weight ratios 8:2 to 2:8 showed that the materials melted together at a lower temperature than the individual components (Supplementary data 2), demonstrating that they are miscible or partially miscible in the liquid state [28].

Supplementary data 2: DSC thermograms of the BUD/AMB-HCl physical mix of the raw materials.

The thermograms of formulations C1 to C8 (Fig. 6B) did not display a visible T_g . For all these systems, DSC scans displayed one broad or two merged exotherms above 110°C followed by one or two endotherms. The endotherms were either merged or isolated with their temperature onsets and ΔH varying depending on the BUD:AMB-HCl ratio, as reported in the Supplementary data 2.

Additionally, scans of C1 presented two small endotherms having a T_{onset} at 90 and 98°C.

Results of the particles' content analysis obtained by HPLC are shown in Table 2. For all formulations, the percentage of drugs found was close to that calculated on the basis that all the $(\text{NH}_4)_2\text{CO}_3$ was eliminated. Also the relative amount of AMB-HCl plus BUD was close to 100%, suggesting that most of the $(\text{NH}_4)_2\text{CO}_3$ was eliminated during the spray drying, and that the particles are mainly composed of BUD and AMB-HCl.

Table 3: Measured and theoretical content of BUD and AMB-HCl in the spray dried particles ($n=3 \pm \text{SD}$). Theoretical contents of drugs in the different formulations were calculated on the basis that: (a) all or (b) none of the $(\text{NH}_4)_2\text{CO}_3$ was eliminated during the spray drying process. NA (Non Applicable)

	BUD			AMB-HCl		
	Theo. cont. (w/w) (a)	Theo. cont. (w/w) (b)	Measured conc. (w/w)	Theo. conc. (w/w) (a)	Theo. conc. (w/w) (b)	Measured conc. (w/w)
C1	94	80	96.83±2.31	6	5	6.10±0.15
C2	88	75	87.42±3.91	12	10	11.55±0.55
C4	76	65	81.66±2.24	24	20	24.25±1.37
C5	86	65	89.73±3.81	14	10	14.53± 0.21
C6	84	55	82.97±2.61	15	10	14.35±0.67
C7	69	45	71.19±2.28	30	20	28.08±0.52
A3	NA	80	82.2±1.5	NA	20	17.8±1.5
A2	NA	90	94.6±1.8	NA	10	5.7±2.9
A1	NA	95	97.1±1.9	NA	5	3.7±1.2

Cumulative mass depositions of selected formulations versus ECD of each ACI stage are shown in Fig. 7. Formulation A1 was composed of particles with MMAD value corresponding to high lung alveoli delivery efficiency ($2.2 \pm 0.21 \mu\text{m}$) and had a high FPF ($72.3 \pm 2.5\%$). The addition of 15% (w/w) of $(\text{NH}_4)_2\text{CO}_3$ (C1) significantly reduced the MMAD to $1.87 \pm 0.22 \mu\text{m}$ and significantly increased the FPF ($84.0 \pm 2.6\%$) (*t-test*, $p < 0.05$). A further increase in AMB-HCl and

(NH₄)₂CO₃ concentration (C5) produced particles with higher MMAD (3.18±0.28 μm) but having a narrow diameter distribution (GSD of 1.79±0.03) and high FPF (74.0±2.5%).

Figure 7: Cumulative particles mass (%) versus the effective cut-off diameter (ECD) of each ACI stages.

Apparent permeability values of BUD, AMB-HCl and fluorescein measured across AIC grown Calu-3 cell monolayers are displayed in Fig. 8. The P_{app} value of BUD across mucus secreting cell monolayer (i.e., $4.5 \pm 0.3 \cdot 10^{-6}$ cm/s) was 1.3-times significantly higher in the presence of 20 μg/mL of AMB-HCl in the apical compartment (i.e., $5.8 \pm 0.4 \cdot 10^{-6}$ cm/s) (*t-test*, $P < 0.05$). Comparable results were obtained when BUD P_{app} value was evaluated after co-processing BUD with AMB-HCl and (NH₄)₂CO₃ (C5). Based on the particle composition analysis, the apical AMB-HCl concentration in this condition was approximately 3.3 μg/mL. Fluorescein P_{app} values showed similar changes as in the case of BUD. In the presence of BUD alone, the fluorescein P_{app} value was $1.4 \pm 0.1 \cdot 10^{-7}$ cm/s and significantly increased to $2.6 \pm 0.6 \cdot 10^{-7}$ cm/s in the presence of formulation C5 (*t-test*, $P < 0.05$). AMB-HCl P_{app} values were identical for all the AMB-HCl concentrations used ($\sim 1.4 \pm 0.2 \cdot 10^{-5}$ cm/s).

Figure 8: BUD, AMB-HCl and fluorescein apical-to-basal P_{app} values measured across Calu-3 cell monolayers. Under all conditions the apical BUD concentration was 20 μg/mL. ($n = 3$, *t-test* * $P < 0.05$).

Apparent permeability values of BUD measured across AIC or LCC grown Calu-3 cell monolayers, with or without AMB are displayed in Fig. 9. The P_{app} value of BUD across LCC grown Calu-3 monolayer (i.e., $9.3 \pm 0.4 \cdot 10^{-6}$ cm/s) was 1.4-times significantly higher than across AIC grown mucus secreting Calu-3 cell monolayer (i.e., $6.8 \pm 0.1 \cdot 10^{-6}$ cm/s) ($p < 0.001$). The addition of AMB in the apical compartment significantly ($P < 0.05$) increased the BUD

permeability across AIC grown Calu-3 cell monolayer, but did not significantly change the BUD permeability across the LCC grown Calu-3 monolayer

Figure 9: BUD apical-to-basal P_{app} values measured across Calu-3 cell monolayer cultured at an air-interfaced culture (AIC) and at a liquid-covered culture (LCC) conditions, with and without AMB-HCl. Under all conditions apical BUD concentration was 20 $\mu\text{g/mL}$. The values represent means \pm SD (n = 3, t-test * $P < 0.05$ and * $P < 0.001$).**

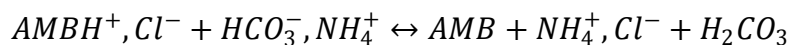
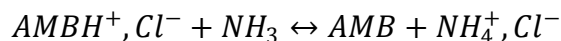
4. Discussion

In order to increase BUD diffusion within abnormally viscous mucus, the co-administration of BUD and AMB-HCl as a dry powder is of interest. Therefore, our studies aimed to develop highly respirable nanoporous microparticles made of BUD and AMB-HCl. These composite particles were formulated with the aim of enhancing BUD diffusion within thick mucus for a local action and not for a bi-therapy purpose or to enhance BUD systemic absorption. Inhalation therapy results in a high concentration of active drug at the site of action and requires much lower doses than oral administration. As shown by Ren *et al.*, [23], this is the case for AMB. Therefore, the drug ratios in the present particle compositions were lower than the doses normally used for the individual drugs when used in oral delivery.

We previously described the formulation of nanoporous microparticles (NPMPs) of pure BUD by spray drying solutions with a solvent made of ethanol and water in a ratio of 80:20 (v/v) [11]. The BUD NPMPs formulated in this previous study were shown to be optimal for pulmonary administration using a DPI as they had high FPF ($74.9 \pm 3.5\%$) and good MMAD ($2.05 \pm 0.10 \mu\text{m}$). However, particles of BUD containing 5 to 20% (w/w) of AMB-HCl prepared in the current work were non-porous and had smooth surfaces (Fig. 1). Particles containing 20 wt% of AMB-HCl (A3) were similar to those obtained by Ren *et al.*, [29] by spray drying an aqueous solution of pure AMB-HCl. The change in BUD particle morphology induced by the addition of AMB-HCl could be due to the slow solidification of AMB-HCl during the solvent evaporation process in the spray dryer. This morphology change was unsatisfactory, as it may adversely affect the particles aerodynamic properties [30, 31]. Thus, $(\text{NH}_4)_2\text{CO}_3$ was incorporated in the formulation in order to overcome this drawback. In fact, $(\text{NH}_4)_2\text{CO}_3$ is commonly used as a blowing agent, [7, 32], pore-forming agent [32] or process enhancer [10, 11]. This compound decomposes and produces gases during spray drying, thus it is able to create porous or hollow particles.

Most of the composite particles made of BUD and AMB-HCl, formulated with $(\text{NH}_4)_2\text{CO}_3$ were porous (Fig. 2). The size and number of pores depended on the initial concentration of AMB-HCl and $(\text{NH}_4)_2\text{CO}_3$ in the spray dried solution. The increase in porosity and the enlargement of the pore size with the increase in $(\text{NH}_4)_2\text{CO}_3$ content may be related to the increase in the amount of CO_2 and NH_3 produced from $(\text{NH}_4)_2\text{CO}_3$ [7]. For AMB-HCl contents <15% (w/w) and $(\text{NH}_4)_2\text{CO}_3$ contents <25% (w/w), the microparticle morphology was similar to that of the pure BUD particles formulated by Nolan *et al.* [11]. However, Nolan *et al.* showed that $(\text{NH}_4)_2\text{CO}_3$ did not have any influence on the pure BUD particle morphology produced in these conditions. In fact, NPMPs of BUD are produced due to the early BUD precipitation in the spray droplet and the formation of gas bubbles do not change their structure [11]. Thus, the formation of nanopores in the BUD/AMB-HCl composite particles, by the addition of $(\text{NH}_4)_2\text{CO}_3$, should be related to its effect on AMB-HCl.

Additionally to its capacity to decompose into gases upon heating, $(\text{NH}_4)_2\text{CO}_3$ dissolved in water produces a solution composed of HCO_3^- , NH_4^+ and NH_3 , with a pH around 9.2. AMB is a weak base having a pKa of 8.05 at 25°C [33]. As a hydrochloride salt, AMB-HCl can react with the HCO_3^- and NH_3 species leading to the formation of AMB base, NH_4^+ , Cl^- and H_2CO_3 as described by the following chemical equilibria.

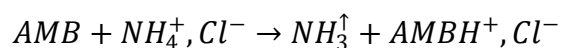


Using the pKa, the relative concentrations of the different species in solution, and considering the medium as pure water, the percentage of AMB in unionised form (base) calculated ranged from 91.8 to 88% of the whole AMB for C1 and C4, respectively. These calculations were performed considering pure aqueous solutions. However, spray dried solutions were made with 80 %v/v of

ethanol. Ethanol is an amphiprotic solvent like water, but having a lower dielectric constant [34]. The apparent ionization constants (pKa) of base, such as ambroxol, in organic solvent:water mixtures decrease with an increase in organic solvent concentration [35]. Therefore, in the presence of ethanol the chemical reactions described above should be favoured, leading to the formation of AMB base more than in pure water.

To support this, DSC scans of a AMB-HCl/(NH₄)₂CO₃ 3/7 (w/w) spray dried system (Fig. 4) and of the formulation C1 (Fig. 6) showed 4 endotherms. The first endotherm, with a temperature onset of 60°C may correspond to solvent evaporation. As observed by Caira *et al.*, [36] the following two endotherms having a T_{onset} at 90 and 98°C are attributed to the melting of the AMB base crystallised as form I and form II, respectively. Furthermore, XRD patterns of AMB-HCl and BUD-AMB-HCl formulations spray dried with (NH₄)₂CO₃ presented a Bragg peak of diffraction at $2\theta = 32.65^\circ$ and at $2\theta = 22.85^\circ$ (Fig. 5). These peaks characterised the presence of NH₄Cl in the particles [37], produced by the reaction of AMB-HCl with (NH₄)₂CO₃. In fact the melting temperature of NH₄Cl is 338°C, thus any residual solid NH₄Cl cannot be eliminated during the spray drying process.

However, the last endotherm observed on DSC scans performed after spray drying AMB-HCl in the presence of (NH₄)₂CO₃ (Fig. 4), having an onset at 229°C, may correspond to the melting of AMB-HCl. This endotherm had a lower temperature onset than the endotherm corresponding to the melting of the pure AMB-HCl, as the melting of AMB-HCl occurred in the liquid AMB base, lowering its chemical potential. This AMB-HCl could result from the re-protonation of AMB base during the spray drying process as described by the following chemical equation.



The re-protonation of AMB base to form AMB-HCl in the BUD/AMB composite formulation

made by spray drying solutions containing $(\text{NH}_4)_2\text{CO}_3$ was also observed. The endotherms corresponding to AMB base were not observed in the DSC scans recorded for formulations other than C1. Furthermore, DSC scans recorded for some formulations displayed two merged exotherms followed by two endotherms, suggesting the recrystallisation and the subsequent melting of 2 materials (BUD and AMB-HCl). Additionally, the PXRD patterns of pure AMB-HCl spray dried in the presence of $(\text{NH}_4)_2\text{CO}_3$ and those of the formulations showed a diffuse halo centred between $2\theta = 15\text{--}22.5^\circ$ (Fig. 5) suggesting the presence of amorphous AMB-HCl.

It appears that the presence of AMB base mixed with BUD during the spray drying process was necessary to formulate nanoporous microparticles. AMB base is less polar than the hydrochloride form and should behave similarly to BUD. During the evaporation process in the spray dryer, the water/ethanol proportion in the solvent droplets should increase as ethanol is more volatile than water. This should induce the nanoprecipitation of BUD, as its water solubility is low [11]. Also, the early BUD nanoprecipitation that occurs in the sprayed droplets, leading to the formation of NPMPs [11], could also occur with the AMB base and not with the AMB-HCl, explaining the difference in the morphology of the BUD-AMB-HCl particles formulated with and without $(\text{NH}_4)_2\text{CO}_3$. The early nanoprecipitation of AMB base could act as seeds to trigger the AMB-HCl solidification.

The reconversion of AMB base to AMB-HCl salt during the spray drying process is an advantageous point in relation to the solubility and potentially the bioavailability of AMB. Similarly, BUD and AMB-HCl were amorphous in the particles formulated with or without $(\text{NH}_4)_2\text{CO}_3$, which also may lead to an improvement of their solubility, dissolution rate and thus, diffusion in thick mucus. Amorphous materials can often be considered as undesirable for pharmaceutical development, mainly because of the concern about their physical stability; however, Nolan *et al.* [11] demonstrated that amorphous particles of BUD were stable up to 1

year at 25°C and 60% RH.

The aerodynamic properties of various types of BUD-AMB-HCl composite particles tested (A1, C1, C5) were satisfactory. In fact, their MMADs were in the 1-5 μm aerodynamic diameter range, which may lead to deep alveolar lung deposition [1, 38, 39]. These MMADs were in the same range as those of pure BUD NPMP prepared and analysed under similar conditions (using an identical impactor, flow rate and inhaler) by Nolan *et al.* [11]. These MMAD values of the BUD-AMB-HCl composite particles were lower than the values measured for the particles made of pure AMB-HCl [29]. Furthermore, the FPF of these composite particles were higher than that obtained for the pure BUD NPMP ($68.69 \pm 1.33\%$) prepared by Nolan *et al.* [11].

For the same initial amount of AMB-HCl of 5% (w/w), the addition of $(\text{NH}_4)_2\text{CO}_3$ decreased the MMAD and significantly increased the FPF from $72.3 \pm 2.5\%$ (A1) to $84.0 \pm 2.6\%$ (C1) (Fig. 7). Thus, the formulation of nanoporous particles improved the particles' aerodynamic properties. An increase in the AMB-HCl content to 14% (w/w) (C5) led to an increase in the MMAD, although it remained in the favourable 1 to 5 μm diameter range. Interestingly, the FPF remained high ($74.0 \pm 2.5\%$) which could be attributed to the low GSD (1.79 ± 0.03) of this system. This narrow aerodynamic particles diameter distribution may presumably result in a good reproducibility in the dose administered to the patient, which is one of the weak points of drug administration by DPI [1]. Also, the FPF of the BUD-AMB-HCl composite particles was higher than that reported by Ren *et al.* [29], who obtained a FPF of 30.93% for particles composed of AMB-HCl/leucine/mannitol in a 2.5/0.5/1 weight ratio and made by spray drying.

In a number of pulmonary diseases, such as cystic fibrosis, patients develop abnormally thick mucus which is responsible for the low diffusion and poor efficacy of drugs [5, 18, 19]. The co-administration of BUD together with AMB-HCl, a mucokinetic, could improve BUD diffusion within the lung and thus increase BUD efficacy.

AMB-HCl is a mucokinetic and influences the rheological properties of the airway fluid by acting directly on epithelial cells [21], for example by modulating their ions secretion [22, 40]. To assess the effect of AMB on BUD diffusion within mucus, different transport experiments across Calu-3 cell AIC cultured monolayers, a model of mucus-producing epithelium [26, 27], were carried out (Fig. 8 and Fig. 9). In fact, AMB was previously shown to act on the ions secretion of Calu-3 cell monolayers, controlling the mucus viscosity [22]. Albeit Calu-3 secretions are probably different from the highly viscous mucus in cystic fibrosis or COPD, measures of BUD permeability could be used as an indirect evaluation of its diffusion within mucus, if the diffusion within the mucus is the limiting factor to the transport across the monolayer. This model was also used to determine if AMB can enhance BUD diffusion through mucus when co-administered. AMB apical-to-basal P_{app} values across Calu-3 cell AIC cultured monolayers ($1.4 \pm 0.1 \cdot 10^{-5}$ cm/s) were constant for the different AMB-HCl concentrations tested (3, 6 and 20 $\mu\text{g/mL}$). This value was close to P_{app} values found for AMB transport across the Caco-2 cell monolayers (i.e., $3.8 - 4.6 \cdot 10^{-5}$ cm/s) [41], a model in which a mucus layer is absent [42]. The authors of this study reported that the permeability of AMB was independent of concentration over a wide concentration range (38 – 380 $\mu\text{g/mL}$) [41]. The consistency of AMB P_{app} values at different concentrations, cell type and the presence of mucus could be due to the relatively high permeability of the drug (i.e., $> 1 \cdot 10^{-5}$ cm/s), making it less sensitive to the viscosity change and suggesting that the AMB diffusion is not limiting its transport across the cell monolayer.

To determine if the mucus is limiting the BUD transport across Calu-3 cell monolayers, BUD permeability was measured across AIC cultured and LCC cultured Calu-3 cell monolayers. In this latter condition, the mucus is highly diluted and cells produce less glycoprotein compared to AIC grown cells [43]. In LCC conditions, a BUD apical-to-basal P_{app} of $9.3 \pm 0.4 \cdot 10^{-6}$ cm/s was determined, which was close to the value of $15 \cdot 10^{-6}$ cm/s measured in previous transport studies

across LCC cultured Calu-3 [27]. In AIC conditions (BUD $C_a = 20 \mu\text{g/mL}$; $t = 180 \text{ min}$), BUD apical-to-basal P_{app} values (i.e., $4.5 \pm 0.3 \cdot 10^{-6}$ to $6.8 \pm 0.1 \cdot 10^{-6} \text{ cm/s}$) were significantly ($P < 0.001$) lower than in LCC conditions and similar to those reported by Borchard *et al.* [26] (i.e., $5.33 \pm 0.95 \cdot 10^{-6} \text{ cm/s}$) under comparable conditions (BUD $C_a = 6.5 - 21.5 \mu\text{g/mL}$; $t = 120 \text{ min}$). Grainger *et al.* [43] have shown that the Calu-3 membrane integrity was higher when grown under LCC conditions compared to AIC conditions. For example, cells cultured using LCC exhibited higher expression levels of ZO-1 protein than the AIC counterpart and the P_{app} value of the fluorescein was significantly lower across LCC than AIC cultured monolayers treated similarly [43]. Also, the decrease in BUD apical-to-basal P_{app} observed in the presence versus the absence of mucus suggests that the diffusion of BUD within this mucus limits its transport across Calu-3 and that the permeability change can be attributed to a change in BUD diffusion.

The addition of AMB-HCl at $20 \mu\text{g/mL}$ or at $3 \mu\text{g/mL}$, when co-formulated by spray drying with BUD, significantly increased the P_{app} of BUD across non-washed AIC cultured Calu-3 cell monolayers. The effect of AMB-HCl was also observed from the fluorescein P_{app} , which was significantly increased in the presence of AMB in comparison to its value measured in the presence of BUD alone. To verify that the increase in BUD permeability observed in the presence of AMB across AIC cultured Calu-3 monolayers was due to a decrease in mucus viscosity and not to an alteration of the membrane integrity caused by the AMB, BUD permeability across LCC grown monolayer was also determined in the presence of AMB. No significant differences were observed for the BUD permeability across LCC grown Calu-3 monolayers in the presence versus the absence of AMB (Fig. 9). This demonstrated that the AMB was able to increase the BUD diffusion within the Calu-3 mucus. Therefore, BUD efficacy should be increased after inhalation of these BUD-AMB hybrid particles in patients having abnormally viscous mucus such as in the case of cystic fibrosis. However, it must be noted that the significant increase of

BUD permeability induced by the AMB was only 1.3-fold. In order to increase this gain in BUD diffusion, other mucoactive agents which act quickly and directly on the mucus, such as mucolytics (N-acetylcysteine) could be investigated and combined with BUD to formulate hybrid particles.

5. Conclusions

With the aim of enhancing budesonide efficacy in the lung of patients suffering from abnormally thick mucus, we developed budesonide-ambroxol hydrochloride hybrid nanoporous microparticles for pulmonary administration by powder inhalation. These hybrid particles were formulated by using $(\text{NH}_4)_2\text{CO}_3$ to obtain nanopores. They showed excellent aerodynamic properties with MMAD ranging from 1.87 to 3.18 μm and FPF higher than 72%. These particles were able to significantly improve budesonide apparent permeability in an *in vitro* model of mucus-producing respiratory epithelium, and should be able to enhance budesonide diffusion within the abnormally thick mucus of cystic fibrosis patients. The formulation of hybrid nanoporous microparticles containing a mucokinetic, such as ambroxol hydrochloride, could also be of interest for other drugs such as antibiotics, in order to treat bacteria protected in thick mucus or biofilms.

References

- [1] E.M. Westerman, P.P.H. Le Brun, D.J. Touw, H.W. Frijlink, H.G.M. Heijerman, Effect of nebulized colistin sulphate and colistin sulphomethate on lung function in patients with cystic fibrosis: A pilot study, *Journal of Cystic Fibrosis*, 3 (2004) 23-28.
- [2] M.B. Dolovich, R. Dhand, Aerosol drug delivery: Developments in device design and clinical use, *The Lancet*, 377 (2011) 1032-1045.
- [3] F.P. Maesen, G. Nakratzas, T.A. Bantje, J. Prins, P.G. Zweers, Formoterol suspension aerosol. Comparison with formoterol solution aerosol for 12 weeks in asthmatic patients, *Chest.*, 102 (1992) 1544-1549.
- [4] V. Petraitis, R. Petraitiene, W.W. Hope, J. Meletiadis, D. Mickiene, J.E. Hughes, M.P. Cotton, T. Stergiopoulou, M. Kasai, A. Francesconi, R.L. Schaufele, T. Sein, N.A. Avila, J. Bacher, T.J. Walsh, Combination Therapy in Treatment of Experimental Pulmonary Aspergillosis: In Vitro and In Vivo Correlations of the Concentration- and Dose- Dependent Interactions between Anidulafungin and Voriconazole by Bliss Independence Drug Interaction Analysis, *Antimicrob. Agents Chemother.*, 53 (2009) 2382-2391.
- [5] Y. Yang, M.D. Tsifansky, C.J. Wu, H.I. Yang, G. Schmidt, Y. Yeo, Inhalable antibiotic delivery using a dry powder co-delivering recombinant deoxyribonuclease and ciprofloxacin for treatment of cystic fibrosis, *Pharmaceutical Research*, 27 (2010) 151-160.
- [6] M. Kumon, P.C.L. Kwok, H. Adi, D. Heng, H.K. Chan, Can low-dose combination products for inhalation be formulated in single crystalline particles?, *European Journal of Pharmaceutical Sciences*, 40 (2010) 16-24.
- [7] D. Traini, P. Young, P. Rogueda, R. Price, In Vitro Investigation of Drug Particulates Interactions and Aerosol Performance of Pressurised Metered Dose Inhalers, *Pharmaceutical Research*, 24 (2007) 125-135.
- [8] W. Kamin, A. Schwabe, I. Krämer, Inhalation solutions - which one are allowed to be mixed? Physico-chemical compatibility of drug solutions in nebulizers, *Journal of Cystic Fibrosis*, 5 (2006) 205-213.
- [9] M.T. Newhouse, P.H. Hirst, S.P. Duddu, Y.H. Walter, T.E. Tarara, A.R. Clark, J.G. Weers, Inhalation of a dry powder tobramycin PulmoSphere formulation in healthy volunteers, *Chest.*, 124 (2003) 360-366.
- [10] A.M. Healy, B.F. McDonald, L. Tajber, O.I. Corrigan, Characterisation of excipient-free nanoporous microparticles (NPMPs) of bendroflumethiazide, *European Journal of Pharmaceutics and Biopharmaceutics*, 69 (2008) 1182-1186.

- [11] L.M. Nolan, L. Tajber, B.F. McDonald, A.S. Barham, O.I. Corrigan, A.M. Healy, Excipient-free nanoporous microparticles of budesonide for pulmonary delivery, *European Journal of Pharmaceutical Sciences*, 37 (2009) 593-602.
- [12] L.M. Nolan, J. Li, L. Tajber, O.I. Corrigan, A.M. Healy, Particle engineering of materials for oral inhalation by dry powder inhalers. II - Sodium cromoglicate, *International Journal of Pharmaceutics*, 405 (2011) 36-46.
- [13] R. Donnelly, J.P. Seale, Clinical pharmacokinetics of inhaled budesonide, *Clin Pharmacokinet*, 40 (2001) 427-440.
- [14] O.S. Usmani, K. Ito, K. Maneechotesuwan, M. Ito, M. Johnson, P.J. Barnes, I.M. Adcock, Glucocorticoid receptor nuclear translocation in airway cells after inhaled combination therapy, *American Journal of Respiratory and Critical Care Medicine*, 172 (2005) 704-712.
- [15] P.L.P. Brand, Inhaled corticosteroids should be the first line of treatment for children with asthma, *Paediatric Respiratory Reviews*, 12 (2011) 245-249.
- [16] A. Alsaeedi, D.D. Sin, F.A. McAlister, The effects of inhaled corticosteroids in chronic obstructive pulmonary disease: A systematic review of randomized placebo-controlled trials, *American Journal of Medicine*, 113 (2002) 59-65.
- [17] E.H.J. Van Haren, J.W.J. Lammers, J. Festen, H.G.M. Heijerman, C.A.R. Groot, C.L.A. Van Herwaarden, The effects of the inhaled corticosteroid budesonide on lung function and bronchial hyperresponsiveness in adult patients with cystic fibrosis, *Respiratory Medicine*, 89 (1995) 209-214.
- [18] R. Dinwiddie, Anti-inflammatory therapy in cystic fibrosis, *Journal of Cystic Fibrosis*, 4 (2005) 45-48.
- [19] K. Khanvilkar, M.D. Donovan, D.R. Flanagan, Drug transfer through mucus, *Advanced Drug Delivery Reviews*, 48 (2001) 173-193.
- [20] S.L. McGill, H.D.C. Smyth, Disruption of the Mucus Barrier by Topically Applied Exogenous Particles, *Molecular Pharmaceutics*, 7 (2010) 2280-2288.
- [21] D. Paleari, G.A. Rossi, G. Nicolini, D. Olivieri, Ambroxol: A multifaceted molecule with additional therapeutic potentials in respiratory disorders of childhood, *Expert Opinion on Drug Discovery*, 6 (2011) 1203-1214.
- [22] I. Hasegawa, N. Niisato, Y. Iwasaki, Y. Marunaka, Ambroxol-induced modification of ion transport in human airway Calu-3 epithelia, *Biochem Biophys Res Commun*, 343 (2006) 475-482.
- [23] Y.C. Ren, L. Wang, H.B. He, X. Tang, Pulmonary selectivity and local pharmacokinetics of ambroxol hydrochloride dry powder inhalation in rat, *Journal of Pharmaceutical Sciences*, 98 (2009) 1797-1803.
- [24] F. Tewes, L. Tajber, O.I. Corrigan, C. Ehrhardt, A.M. Healy, Development and characterisation of soluble polymeric particles for pulmonary peptide delivery, *Eur. J. Pharm. Sci.*, 41 (2010) 337-352.

- [25] F. Tewes, O.L. Gobbo, M.I. Amaro, L. Tajber, O.I. Corrigan, C. Ehrhardt, A.M. Healy, Evaluation of HP β CD-PEG microparticles for salmon calcitonin administration via pulmonary delivery, *Molecular Pharmaceutics*, 8 (2011) 1887-1898.
- [26] G. Borchard, M.L. Cassar, P.E.H. Roemel, B.I. Florea, H.E. Junginger, Transport and local metabolism of budesonide and fluticasone propionate in a human bronchial epithelial cell line (Calu-3), *Journal of Pharmaceutical Sciences*, 91 (2002) 1561-1567.
- [27] B. Forbes, C. Ehrhardt, Human respiratory epithelial cell culture for drug delivery applications, *European Journal of Pharmaceutics and Biopharmaceutics*, 60 (2005) 193-205.
- [28] V. Caron, L. Tajber, O.I. Corrigan, A.M. Healy, A comparison of spray drying and milling in the production of amorphous dispersions of sulfathiazole/polyvinylpyrrolidone and sulfadimidine/polyvinylpyrrolidone, *Molecular Pharmaceutics*, 8 (2011) 532-542.
- [29] Y. Ren, C. Yu, K. Meng, X. Tang, Influence of formulation and preparation process on ambroxol hydrochloride dry powder inhalation characteristics and aerosolization properties, *Drug Development and Industrial Pharmacy*, 34 (2008) 984-991.
- [30] A.H.L. Chow, H.H.Y. Tong, P. Chattopadhyay, B.Y. Shekunov, Particle engineering for pulmonary drug delivery, *Pharmaceutical Research*, 24 (2007) 411-437.
- [31] T.M. Crowder, J.A. Rosati, J.D. Schroeter, A.J. Hickey, T.B. Martonen, Fundamental effects of particle morphology on lung delivery: Predictions of Stokes' law and the particular relevance to dry powder inhaler formulation and development, *Pharmaceutical Research*, 19 (2002) 239-245.
- [32] D.A. Edwards, J. Hanes, G. Caponetti, J. Hrkach, A. Ben-Jebria, M.L. Eskew, J. Mintzes, D. Deaver, N. Lotan, R. Langer, Large porous particles for pulmonary drug delivery, *Science*, 276 (1997) 1868-1871.
- [33] M. Meloun, T. Syrov, A. Vrana, The thermodynamic dissociation constants of ambroxol, antazoline, naphazoline, oxymetazoline and ranitidine by the regression analysis of spectrophotometric data, *Talanta*, 62 (2004) 511-522.
- [34] G. Akerlof, Dielectric constants of some organic solvent-water mixtures at various temperatures, *Journal of the American Chemical Society*, 54 (1932) 4125-4139.
- [35] K. Takcs-Novk, K.J. Box, A. Avdeef, Potentiometric pKa determination of water-insoluble compounds: validation study in methanol/water mixtures, *International Journal of Pharmaceutics*, 151 (1997) 235-248.
- [36] M.R. Caira, A. Foppoli, M.E. Sangalli, L. Zema, F. Giordano, Thermal and structural properties of ambroxol polymorphs, *Journal of Thermal Analysis and Calorimetry*, 77 (2004) 653-662.

- [37] G.A. Carter, R.D. Hart, M.R. Rowles, C.E. Buckley, M.I. Ogden, The effect of processing parameters on particle size in ammonia-induced precipitation of zirconyl chloride under industrially relevant conditions, *Powder Technology*, 191 (2009) 218-226.
- [38] J.S. Patton, P.R. Byron, Inhaling medicines: Delivering drugs to the body through the lungs, *Nature Reviews Drug Discovery*, 6 (2007) 67-74.
- [39] D.A. Edwards, C. Dunbar, Bioengineering of therapeutic aerosols, in, 2002, pp. 93-107.
- [40] T. Yamada, Y. Takemura, N. Niisato, E. Mitsuyama, Y. Iwasaki, Y. Marunaka, Action of N-acylated ambroxol derivatives on secretion of chloride ions in human airway epithelia, *Biochemical and Biophysical Research Communications*, 380 (2009) 586-590.
- [41] E. Štětinová, L. Smetanová, D. Kholová, Z. Svoboda, J. Květina, Transepithelial transport of ambroxol hydrochloride across human intestinal Caco-2 cell monolayers, *General Physiology and Biophysics*, 28 (2009) 309-315.
- [42] C. Meaney, C. O'Driscoll, Mucus as a barrier to the permeability of hydrophilic and lipophilic compounds in the absence and presence of sodium taurocholate micellar systems using cell culture models, *European Journal of Pharmaceutical Sciences*, 8 (1999) 167-175.
- [43] C.I. Grainger, L.L. Greenwell, D.J. Lockley, G.P. Martin, B. Forbes, Culture of Calu-3 cells at the air interface provides a representative model of the airway epithelial barrier, *Pharm Res*, 23 (2006) 1482-1490.

Table 1: Total content of solids materials (% w/w) used to prepare the feed solutions (1 % w/v).

Compounds	Solid content % (w/w)										
	With (NH ₄) ₂ CO ₃								Without (NH ₄) ₂ CO ₃		
	C1	C2	C3	C4	C5	C6	C7	C8	A1	A2	A3
BUD	80	75	70	65	65	55	45	33	95	90	80
AMB-HCl	5	10	15	20	10	10	20	33	5	10	20
(NH₄)₂CO₃	15	15	15	15	25	35	35	33	0	0	0

Table 2: Geometric volume-weighted particles size analysis

	D₅₀ (μm)	SPAN	Specific Surface Area of particles calculated as smooth spheres (m²/g)
C1	2.4±0.3	1.75±0.05	3.19±0.31
C2	2.6±0.2	1.70±0.1	2.94±0.28
C4	3.0±0.3	2.20±0.15	2.52±0.34
C5	2.6±0.3	1.67±0.09	3.07±0.30
C6	2.8±0.4	1.70±0.15	3.06±0.35
C7	4.6±1.1	2.90±0.62	1.98±0.46

Table 3: Measured and theoretical content of BUD and AMB-HCl in the spray dried particles (n=3 ± SD). Theoretical contents of drugs in the different formulations were calculated on the basis that: (a) all or (b) none of the (NH₄)₂CO₃ was eliminated during the spray drying process. NA (Non Applicable)

	BUD			AMB-HCl		
	Theo. cont. (w/w) (a)	Theo. cont. (w/w) (b)	Measured conc. (w/w)	Theo. conc. (w/w) (a)	Theo. conc. (w/w) (b)	Measured conc. (w/w)
C1	94	80	96.83±2.31	6	5	6.10±0.15
C2	88	75	87.42±3.91	12	10	11.55±0.55
C4	76	65	81.66±2.24	24	20	24.25±1.37
C5	86	65	89.73±3.81	14	10	14.53± 0.21
C6	84	55	82.97±2.61	15	10	14.35±0.67
C7	69	45	71.19±2.28	30	20	28.08±0.52
A3	NA	80	82.2±1.5	NA	20	17.8±1.5
A2	NA	90	94.6±1.8	NA	10	5.7±2.9
A1	NA	95	97.1±1.9	NA	5	3.7±1.2

Figure 1: SEM of particles made of BUD and AMB-HCl as described in Table 1.

Figure 2: SEM and specific surface area values of the particles formulated in presence of $(\text{NH}_4)_2\text{CO}_3$ as described in Table 1. Error bars in the histogram correspond to the standard deviation of the specific surface area values calculated from 3 measurements.

Figure 2: PXRD patterns of the raw and spray dried materials.

Figure 3: DSC thermograms of the unprocessed and spray dried materials. Insert in the figure is a magnified view of the spray dried AMB-HCl thermogram in the region of the T_g .

Figure 4: PXRD patterns of the formulation as described in Table 1.

Figure 6: Thermograms of the powders formulated without (A) and with (B) $(\text{NH}_4)_2\text{CO}_3$.

Figure 7: Cumulative particles mass (%) versus the effective cut-off diameter (ECD) of each ACI stages.

Figure 8: BUD, AMB-HCl and fluorescein apical-to-basal P_{app} values measured across Calu-3 cell monolayer cultured at an air-liquid interface. Under all conditions apical BUD concentration was 20 $\mu\text{g}/\text{mL}$. The values are means \pm SD (n=3, t-test * $P < 0.05$)

Figure 9: BUD apical-to-basal P_{app} values measured across Calu-3 cell monolayer cultured at an air-interfaced culture (AIC) and at a liquid-covered culture (LCC) conditions, with and without AMB-HCl. Under all conditions apical BUD concentration was 20 $\mu\text{g}/\text{mL}$. The values represent means \pm SD (n = 3, t-test * $P < 0.05$ and * $P < 0.001$).**

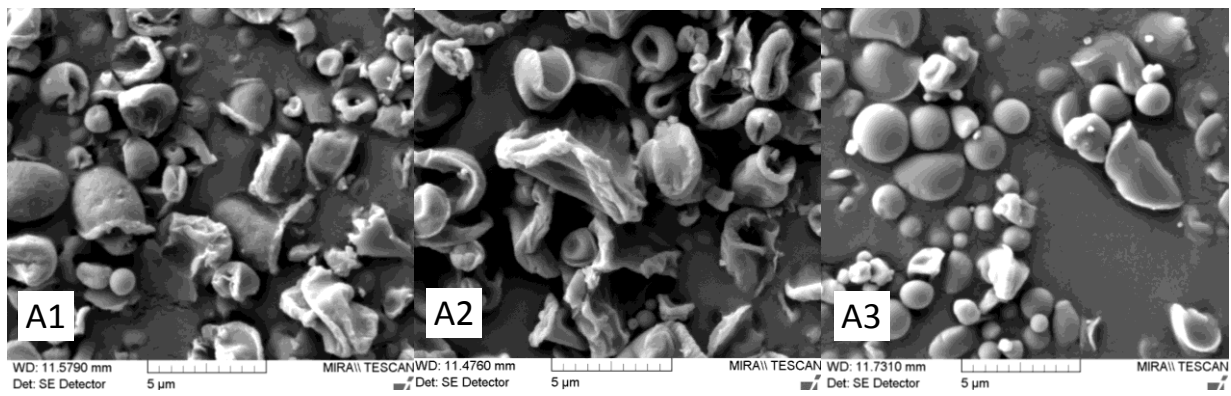


Figure 1: SEM of particles made of BUD and AMB as described in Table 1.

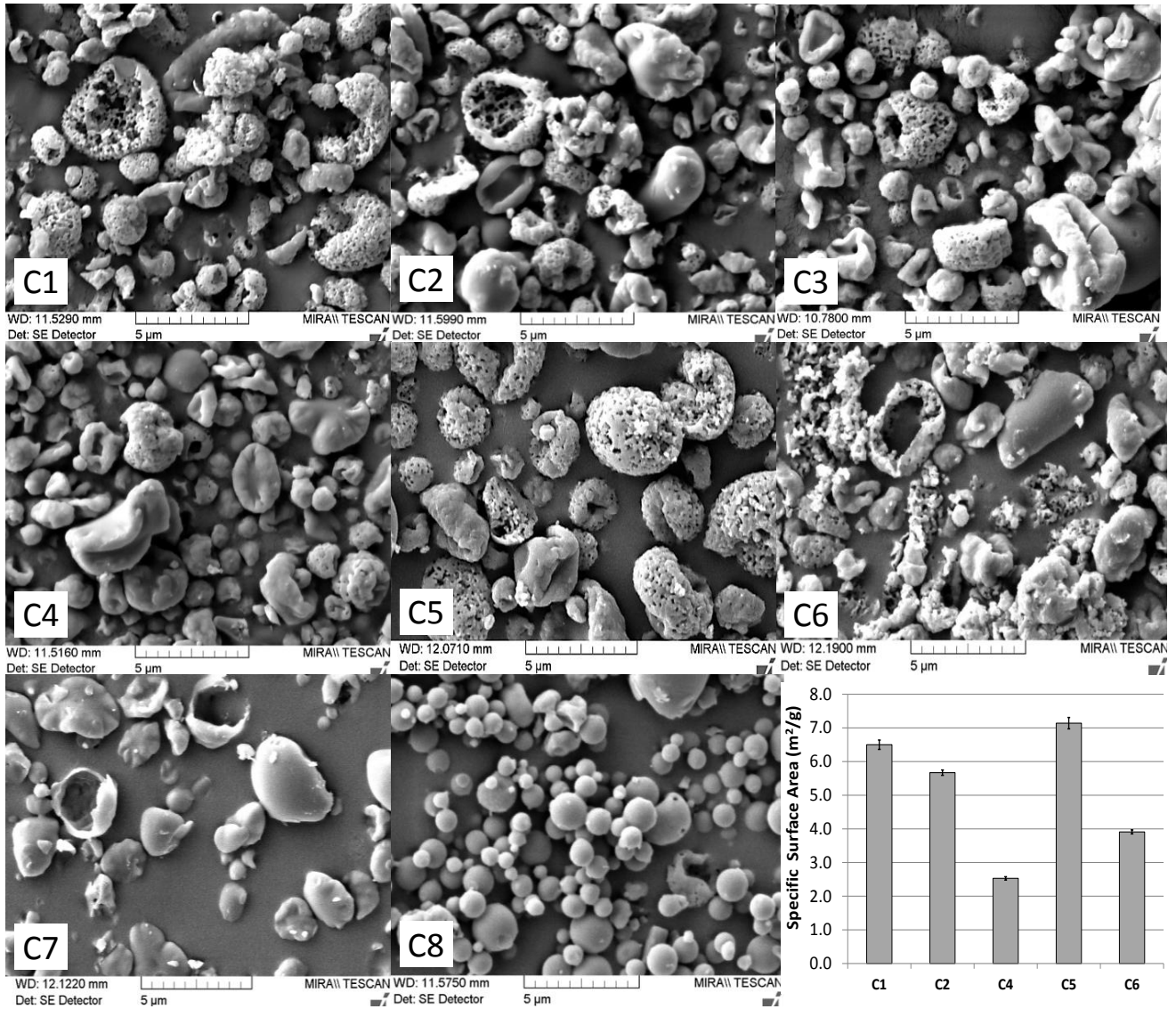


Figure 2: SEM and specific surface area values of the particles formulated in presence of $(\text{NH}_4)_2\text{CO}_3$ as described in Table 1. Error bars in the histogram correspond to the standard deviation of the specific surface area values calculated from 3 measurements

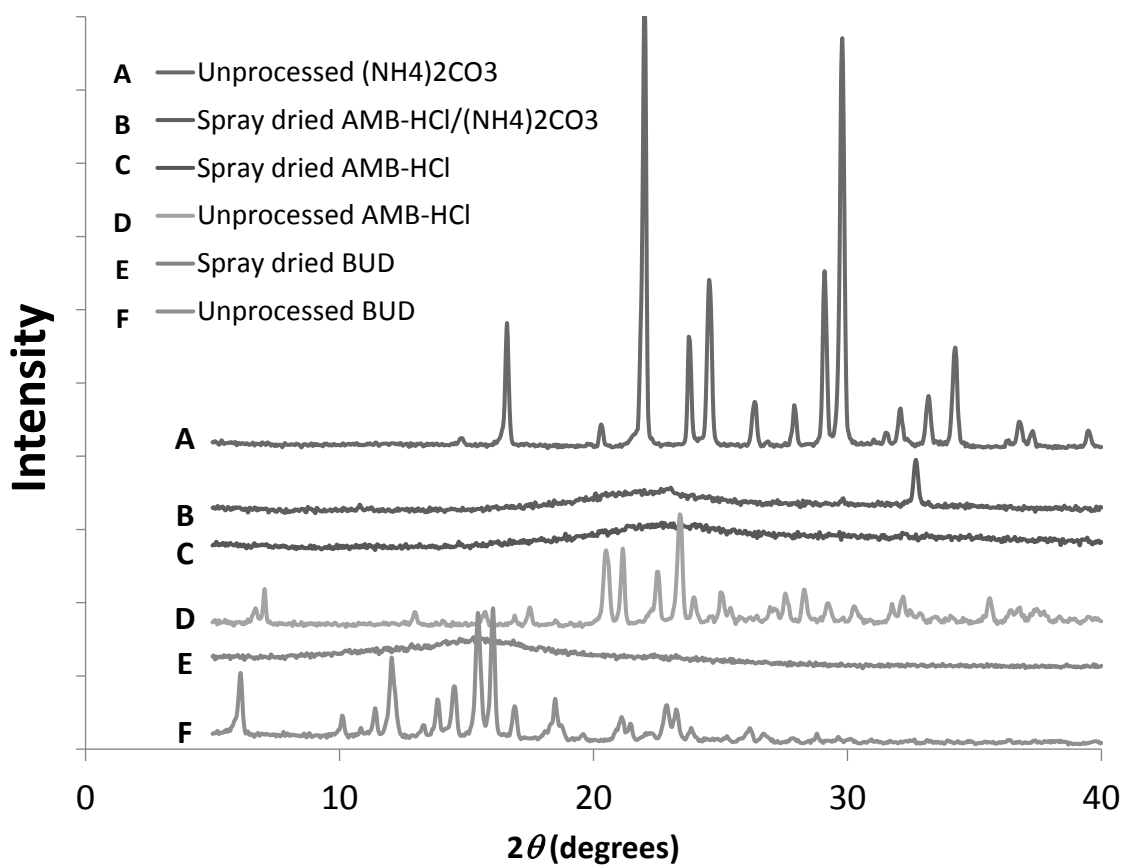


Figure 3: PXRD patterns of the raw and spray dried materials.

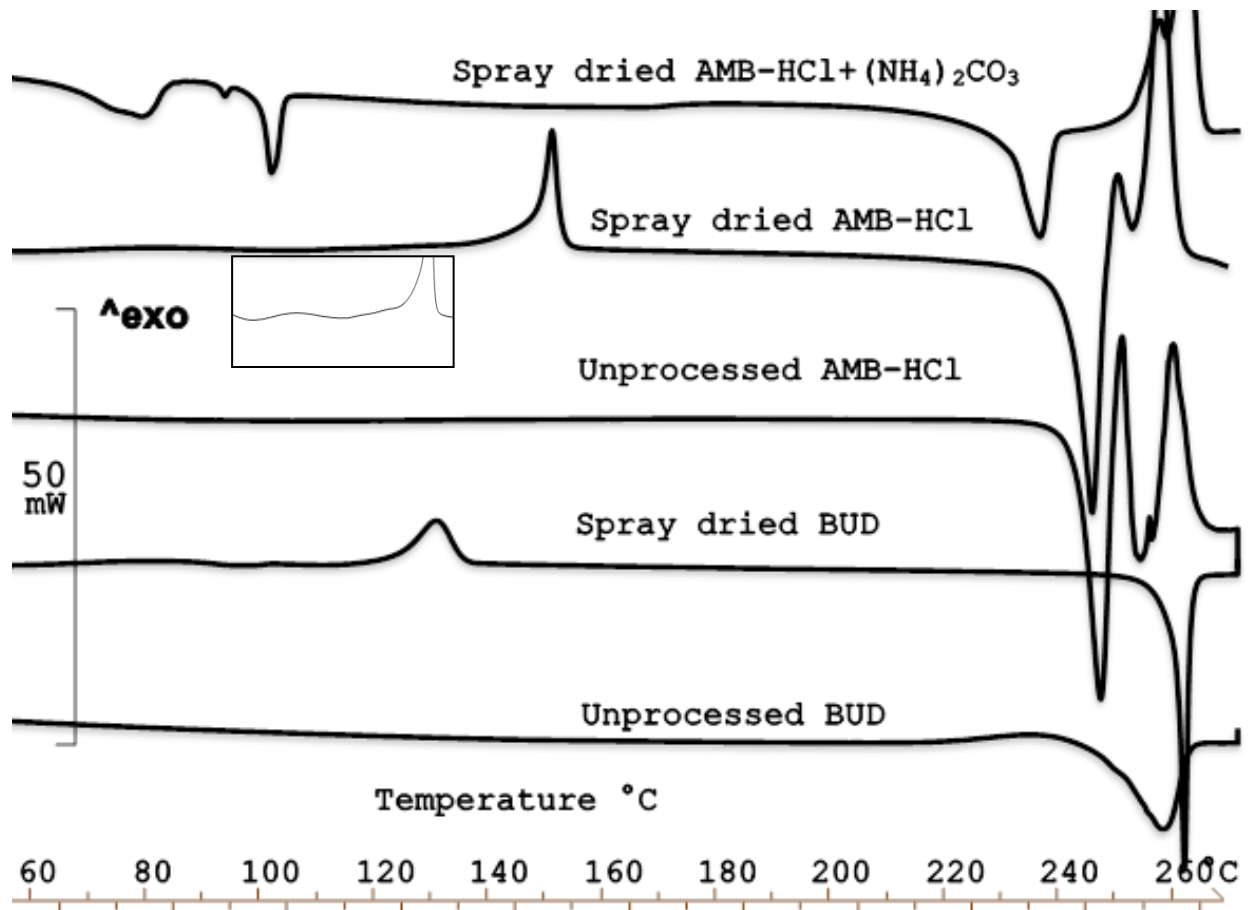


Figure 4: DSC thermograms of the unprocessed and spray dried materials. Insert in the figure is a magnified view of the spray dried AMB-HCl thermogram in the region of the T_g.

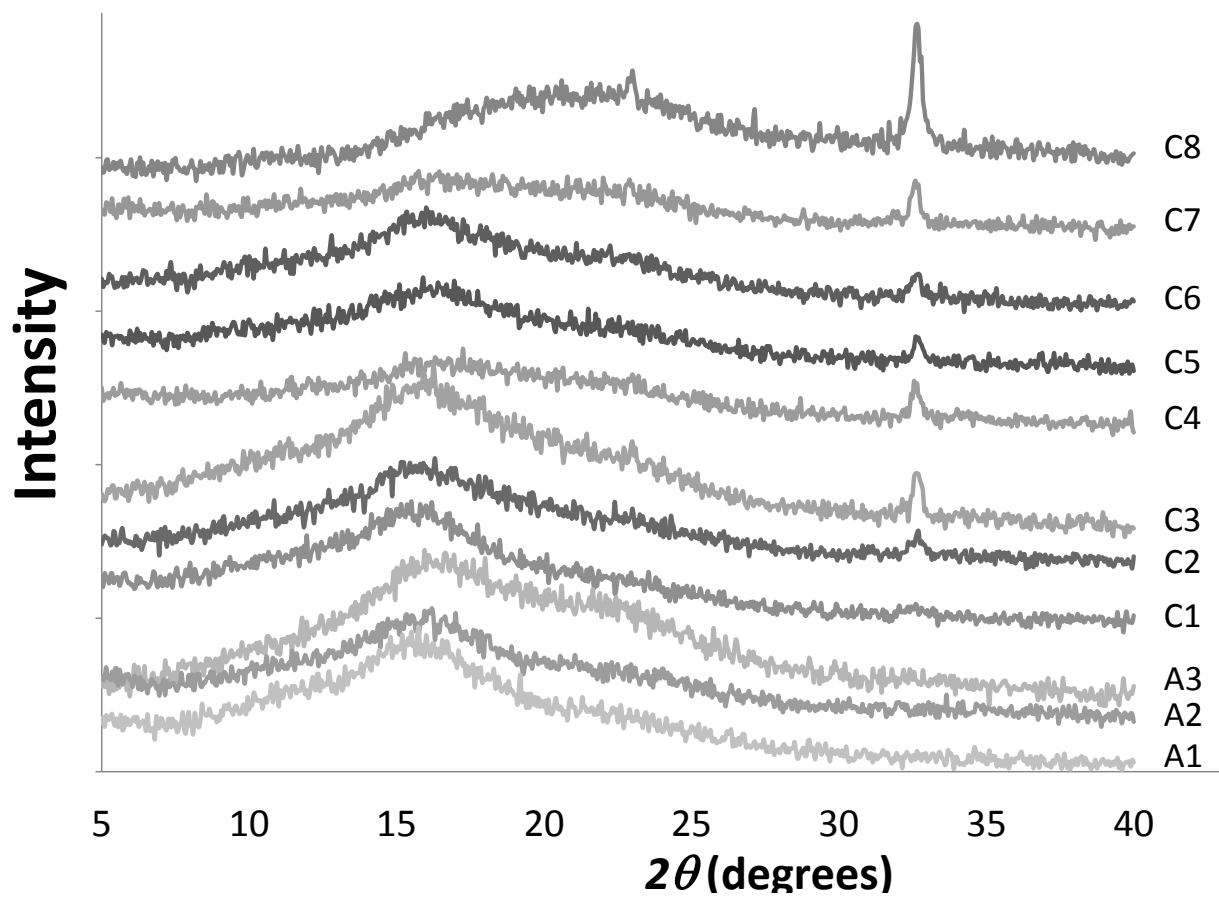


Figure 5: PXRD patterns of the formulation as described in Table 1.

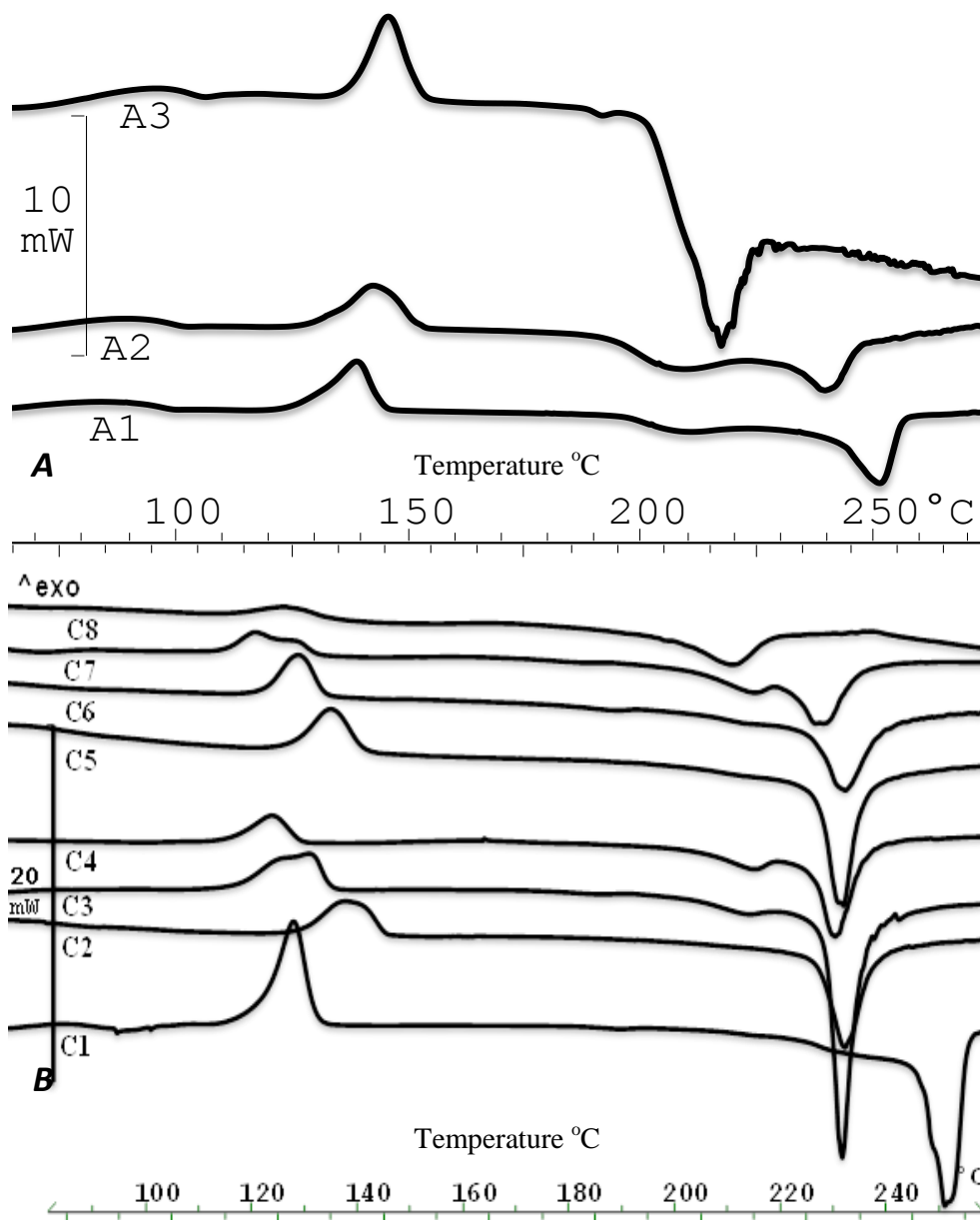


Figure 6: Thermograms of the powders formulated without (A) and with (B) $(\text{NH}_4)_2\text{CO}_3$.

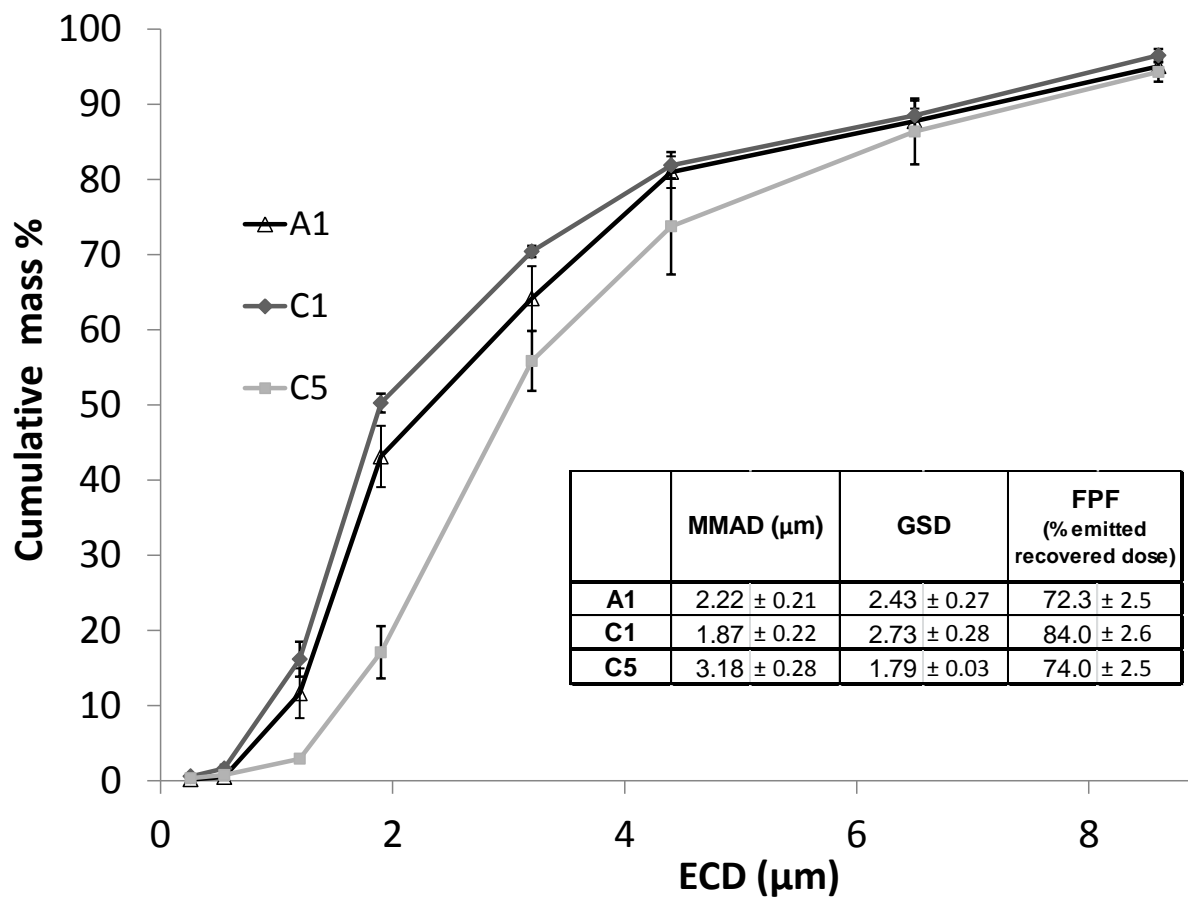


Figure 7: Cumulative particles mass (%) versus the effective cut-off diameter (ECD) of each ACI stages.

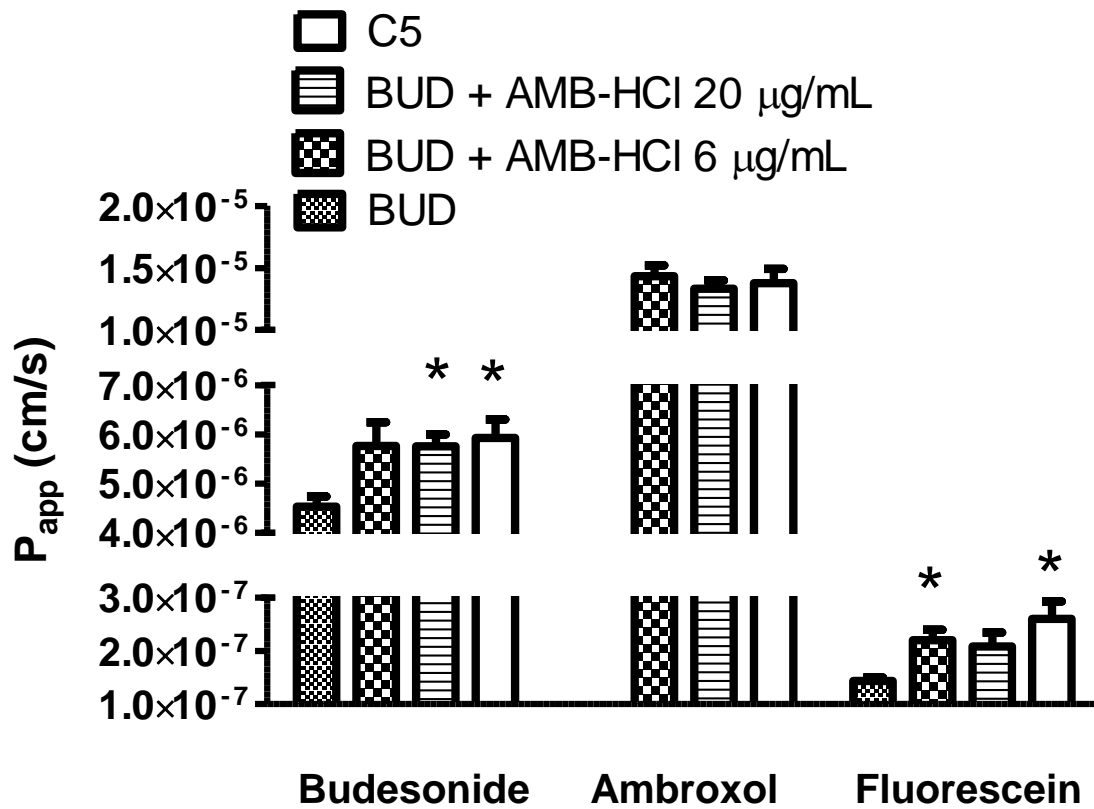


Figure 8: BUD, AMB-HCl and fluorescein apical-to-basal P_{app} values measured across Calu-3 cell monolayer cultured at an air-liquid interface. Under all conditions apical BUD concentration was 20 µg/mL. (n=3, t-test * $P < 0.05$)

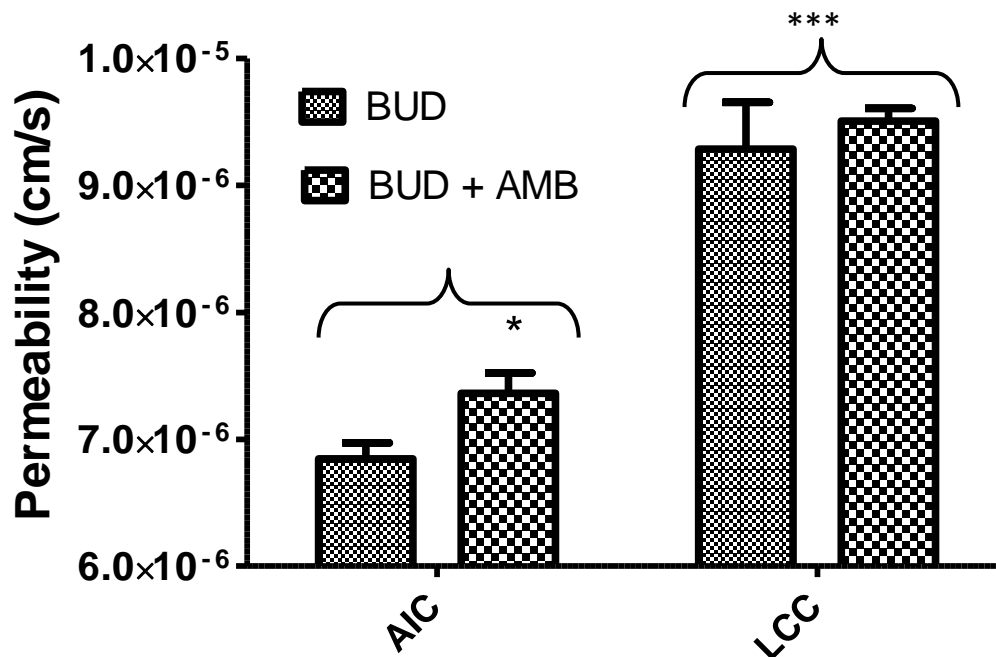


Figure 9: BUD apical-to-basal P_{app} values measured across Calu-3 cell monolayer cultured at an air-interfaced culture (AIC) and at a liquid-covered culture (LCC) conditions, with and without AMB-HCl. Under all conditions apical BUD concentration was 20 $\mu\text{g}/\text{mL}$. The values represent means \pm SD ($n = 3$, t-test * $P < 0.05$ and * $P < 0.001$).**

Supplementary material

[Click here to download Supplementary material: Supplementary AMB-BUD.docx](#)